Evaluation of pinned column base-plate connections in low-rise metal buildings

Aryan, Hadi; Gencturk, Bora; Hosseini, Farshid; Kavoura, Florentia

DOI
10.1007/s11709-025-1167-6

Publication date
2025

Document Version
Final published version

Published in
Frontiers of Structural and Civil Engineering

Citation (APA)
Aryan, H., Gencturk, B., Hosseini, F., & Kavoura, F. (2025). Evaluation of pinned column base-plate connections in low-rise metal buildings. *Frontiers of Structural and Civil Engineering*, *19*(4), 578–597. https://doi.org/10.1007/s11709-025-1167-6

Front. Struct. Civ. Eng. 2025, 19(4): 578–597
https://doi.org/10.1007/s11709-025-1167-6

RESEARCH ARTICLE

Evaluation of pinned column base-plate connections in low-rise metal buildings

Hadi ARYAN[a], Bora GENCTURK[a*], Farshid HOSSEINI[b], Florentia KAVOURA[c]

[a] Sonny Astani Department of Civil and Environmental Engineering, University of Southern California, Los Angeles, CA 90089, USA

[b] TYLin, Irvine, CA 92618, USA

[c] Civil Engineering & Geosciences Department, Delft University of Technology, Delft 2600, Netherlands

[*]Corresponding author. E-mail: gencturk@usc.edu

ABSTRACT In this paper, a computational approach is undertaken to determine the rotational stiffness and moment capacity provided by typical "pinned" column base-plate connections in low-rise metal buildings by analyzing a wide-range of connection parameters. The most influencing details of the connections on the overall behavior were identified. First, development and validation of high-fidelity computational models using experimental data are described. Then, the validated models were used to perform a parametric study to understand the effect of configurational details on the rotational stiffness and moment capacity of the column base-plate connections with anchor rods between the flanges. Anchor rod diameter, by itself, and in combination with base-plate thickness, was found to be the most influential parameter on the moment capacity of connections with smaller web depths. For larger web depths, the number of anchor rods was influential in the moment capacity, particularly, in one of the loading directions.

KEYWORDS low-rise metal buildings, base-plate connection, stiffness, moment capacity

1 Introduction

"Pinned" connections under investigation in this research (Fig. 1(a)) are widely used in gabled frames in low-rise metal buildings (Fig. 1(b)) in the United States. However, there is a lack of understanding of the moment–rotation behavior of these pinned connections, especially, as it relates to selection of the geometric details. The stiffness and strength of the connections under monotonic loading is the main focus of this paper, however, given the nature of modeling and experimental data used to validate the computational models, the results can also be used in the context of seismic effects. Additional consideration to stiffness and strength degradation should; however, be given for interpretation of these results for seismic effects.

Several computational studies have investigated the behavior of column base-plate connections [1–12]. The effect of load eccentricity and the base-plate thickness on the strain distribution within the base-plate was investigated by Thambiratnam and Krishnamurthy [2]. Three-dimensional (3D) finite element models of the column base-plate connections under axial loads and moments were created. It was found that for a constant axial load, the strains increased with decreasing base-plate thickness for high eccentricities. Additionally, the findings supported that the maximum bearing pressure occurs under the compression flange in thinner base-plates and closer to the edge in thicker base-plates.

Hamizi and Hannachi [5] used the experimental data from Picard and Beaulieu [13] to validate their finite element models. In their modeling approach, the nonlinear interaction between the base-plate and the grout was taken into consideration. It was reported that the finite element modeling resulted in lower rotations up to 25% than the ones obtained experimentally. It was also emphasized that the base-plate connections with higher number of anchor rods lead to smaller rotations and

Article history: Received Jan 10, 2024; Accepted Dec 17, 2024

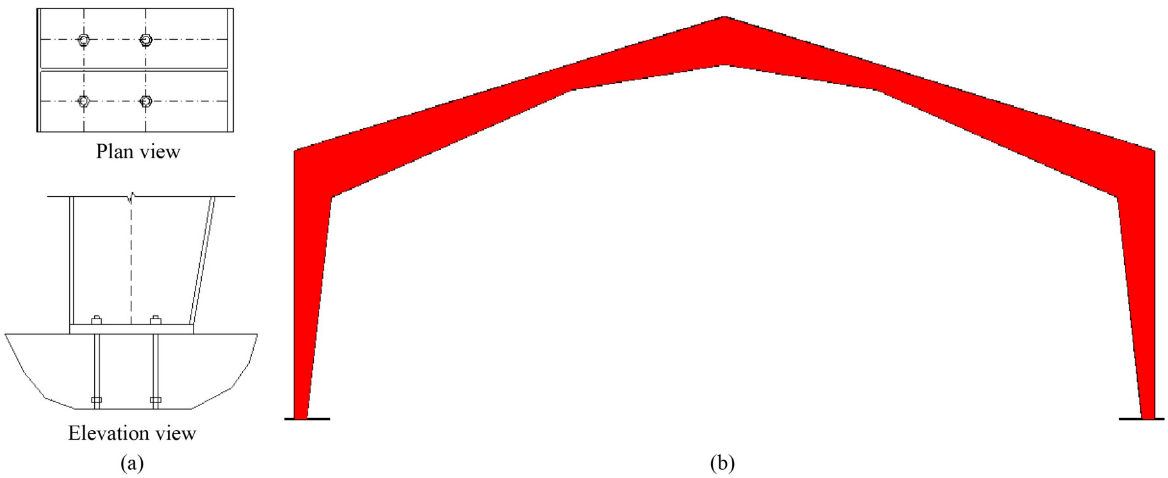

Fig. 1 (a) Pinned base-plate configurations studied in this paper; (b) typical configuration of gabled frames in low-rise metal buildings.

consequently to a higher rigidity. Hamizi and Hannachi [5] also underlined that an increase in the applied axial load from 100 to 600 kN leads to a 30% increase in the degree of fixity of the base-plate connections.

In a study by Bajwa [6], it was found that the lateral displacement of the metal buildings calculated from the computational models resulted in almost double the deflections of those found in the experiments. The most possible source of this difference was identified as the modeling approach for the column to base-plate connection indicating the need for further research in modeling of these connections.

Verma [8] extended the research conducted by Bajwa [6] and focused on partially restrained behavior of base-plate connections conservatively modeled as pinned connections using finite element modeling. It was noted that the pinned connection assumption overestimates the lateral drifts and thus causes larger moments at the knee of the gable frames.

Amaral [9] developed finite element models of column base-plate connections in a commercial finite element modeling package and validated these models using data from the experiments performed by Bajer et al. [14] The models were subjected to uniaxial bending about the strong axis or biaxial bending. The rotational stiffnesses obtained from the finite element models were compared with the ones calculated from the component method described in Eurocode 3 [15]. This comparison revealed that the component method is very conservative in estimating the rotational stiffness of the connections. Additionally, a model for predicting the column base-plate connection behavior under weak axis bending was proposed.

Razzaghi and Khoshbakht [10] created 3D finite element models for evaluating the nonlinear behavior of column base-plate connections. The most influential parameters on the moment capacity and the rotational stiffness of the connections were identified as the base-plate thickness, the anchor rod diameter, and the stiffeners in the connection. It was shown that these parameters affect the moment rotation behavior and stress distribution in addition to the rigidity of the column base-plate connection. Including the fixity of the base-plate connections in the design of steel frames was therefore recommended, which confirms the need for additional research on nominally pinned base-plate connections considered in this study.

Nawar et al. [11] performed a parametric study using finite element modeling to investigate the rotational stiffness, moment resistance, and energy absorption of pinned base-plate connections on reinforced concrete foundations under axial loading and cyclic lateral loading up to 10% story drift. The reference model was a constant I-shape section throughout the height welded to a rectangular base-plate and connected to the foundation with four anchor rods. The studied parameters included the base-plate thickness, anchor rod diameter, number of anchor rods, and the arrangement of the anchor rods. Results identified the diameter and arrangement of the anchor rods as the most influential parameters on the rotational stiffness and moment capacity of the pinned base-plate connections. The effect of the base-plate thickness was not as pronounced as that of the other parameters. Increasing the anchor rod diameter increased the connection moment resistance between 150% to 260% depending on the base-plate thickness. Additionally, at a fixed anchor rod diameter, increasing the base-plate thickness increased the rotational stiffness by up to 53%. The influence of the base-plate thickness on the rotational stiffness reduced when the spacing between the anchor rods was increased.

In this paper, a computational approach was undertaken to analyze a wide-range of pinned base-plate connection parameters. The most influencing details of the connections on the overall behavior were identified. First, high-fidelity computational models were developed and validated using experimental data reported in Kavoura et al. [16–19]. The validated computational models were used to understand the behavior of pinned column base-plate connections in terms of their rotational stiffness, moment capacity and inelastic behavior. Specifically, the base-plate thickness and width, the anchor rod diameter and number of anchor rods, the flange and web thicknesses, and the gage and pitch distances of the anchor rods were studied. The column base-plate connections investigated in this research with tapered-web columns represent most configurations currently used in the metal building industry. To the authors' knowledge, no such comprehensive study exists in literature on these base-plate connections and this paper aims to fill this research gap. The main goal of this research is to provide new understanding and additional data to guide the design codes and provisions for the pinned base-plate connections in metal buildings. It is noted that an evaluation of the existing design guides and recommendations both in terms of the observed failure mechanisms in these pinned base-plate connections and their capacities is presented in detail by the authors in Ref. [17]. In Ref. [17], AISC Steel Construction Manual [20], AISC Design Guides 1 [21], 4 [22], and 16 [23], as well as Eurocode 3 [15] were evaluated for their performance in predicting the behavior of pinned base-plate connections.

2 Summary of experiments used for model validation

The finite element models in this paper were validated using the experimental data presented in Ref. [16]. A representation of the base-plate configurations is shown in Fig. 2, and the parameters of the ten tested base-plate connections are presented in Table 1. The experiments included two groups of specimens each with a specific web depth. The first group had four anchor rods and the second group had six or eight anchor rods. A constant axial loading was applied on top of the columns using two hydraulic jacks. An in-plane cyclic lateral loading was applied at the top of the column using a hydraulic actuator. The main measurements during testing included the in-plane displacements at different elevations of the column using string potentiometers, transfer beam rotation at the top of the column using two string potentiometers, column rotation at the bottom using two string potentiometers, and strains in the base-plate using strain gauges.

3 Modeling approach

Detailed 3D finite element models were created in ATENA 3D [24] to simulate the behavior of the column base-plate connection tests described above. A representative model (for S04 in Table 1) is shown in Fig. 3. Different macro-elements were used for the column stub, base-plate, concrete foundation, connection fixtures and other relevant components of the test. The details of the geometry, loading and boundary conditions, constitutive models, and mesh and contact interactions are presented in the following sections.

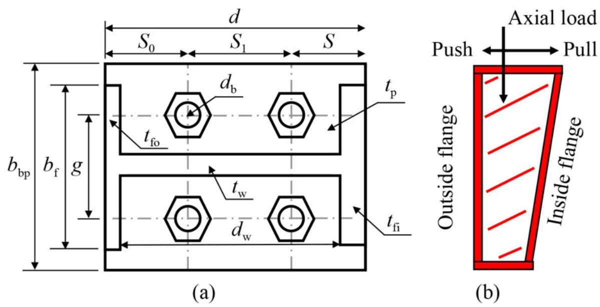

Fig. 2 Typical base-plate connection configuration: (a) base-plate connection details; (b) elevation view of the tested column stubs in Ref. [16].

Table 1 Details of the tested base-plate connections. Data from Ref. [16]

Specimen ID	d_w (mm)	b_f (mm)	t_{fo} (mm)	t_{fi} (mm)	b_{bp} (mm)	d (mm)	t_w (mm)	t_p (mm)	d_b (mm)	g (mm)	S_0 (mm)	S_1 (mm)	S (mm)	No. of anchor rods	Axial load (kN)
S01	304.8	203.2	6.4	9.5	203.2	320.7	4.7	15.9	19.1	101.6	76.2	101.6	158.8	4	222.0
S02	304.8	203.2	6.4	9.5	203.2	320.7	4.7	15.9	19.1	101.6	76.2	152.4	92.1	4	222.0
S03	304.8	203.2	6.4	9.5	203.2	320.7	4.7	15.9	25.4	101.6	101.6	101.6	117.5	4	222.0
S04	304.8	254.0	6.4	9.5	254	320.7	4.7	15.9	31.8	127.0	101.6	127.0	92.1	4	222.0
S05	304.8	254.0	6.4	9.5	254	320.7	4.7	9.5	31.8	127.0	101.6	127.0	92.1	4	222.0
S06	304.8	254.0	12.7	15.9	254	333.4	4.7	15.9	31.8	127.0	101.6	127.0	104.8	4	222.0
S07	558.8	355.6	12.7	15.9	355.6	587.4	6.4	15.9	31.8	127.0	101.6	127.0	231.8	6	445.0
S08	558.8	355.6	12.7	15.9	355.6	587.4	6.4	15.9	31.8	127.0	101.6	127.0	104.8	8	445.0
S09	558.8	355.6	12.7	15.9	355.6	587.4	6.4	15.9	31.8	127.0	101.6	127.0	104.8	8	445.0
S10	558.8	355.6	12.7	15.9	254	587.4	6.4	19.1	31.8	127.0	101.6	127.0	104.8	8	445.0

Note: Refer to Fig. 2 for definitions of the variables. Axial loads correspond to approximately 50% and 100% of the expected service load.

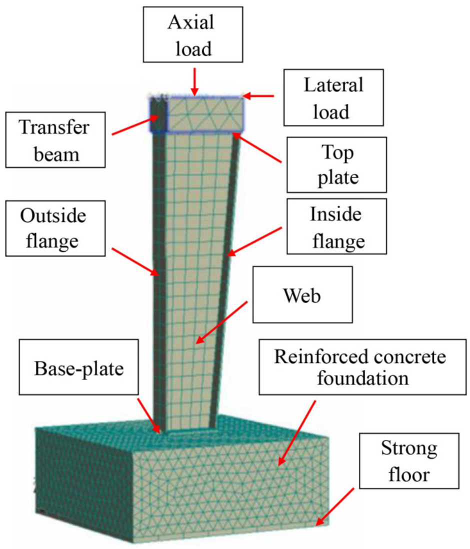

Fig. 3 Detailed 3D finite-element models of column base-plate connection tests.

3.1 Geometry

The geometry of the finite element models was identical to the specimens in the experimental program. The geometric details of the column base-plate connections are given in Table 1 and the relevant dimensions are shown in Fig. 2(a). The specimens were grouped into two main categories based on their web-depths. Specimen 01 (S01) to S06 formed the first group while S07 to S10 formed the second group. The base-plate thickness varied from 9.5 to 19.1 mm while the straight (outside) flange and the tapered (inside) flange thicknesses varied from 6.4 to 12.7 mm and from 9.5 to 15.9 mm, respectively, and the web thickness varied from 4.7 to 6.4 mm. Three different anchor rod diameters were used: 19, 25, and 32 mm, with varying gages, setbacks, and pitches as indicated in Table 1. The effective areas of the 19.1, 25.4, and 31.8 mm diameter anchor rods were 2.138×10^2, 3.801×10^2, and 5.940×10^2 mm^2, respectively. All the first group base-plate connections had four anchor rods while the second group connections had six or eight anchor rods. The reinforced concrete foundation was modeled with the same dimensions as the ones used in the experiments (i.e., 1220 mm × 1220 mm × 457 mm) and connected with a high stiffness plate (1220 mm × 1220 mm × 30 mm), which represented the strong floor in the experiments.

3.2 Loading and boundary conditions

The models were subjected to an axial compressive load and lateral displacements applied through the transfer beam at top of the column (Fig. 3) following the experiment by the authors in Ref. [16]. The height of the transfer beam was represented with half the height of the transfer beam in the experiments using symmetry. Specifically, the lateral load was applied to the transfer beam, 1835 mm above the base of the columns, at 2.5 mm displacement increments (Fig. 3). The compressive axial load was applied as a pressure acting on top of the transfer beam (Fig. 3). The boundary conditions were applied to the strong floor (Fig. 3), which was modeled as a rigid plate with fixed supports at the bottom. The concrete foundation was fixed to the strong floor. No additional boundary conditions were applied to the column, foundation or the transfer beam.

3.3 Constitutive models

The material properties for concrete foundation, steel reinforcement in concrete, steel base-plate, and inside and outside flanges used in the finite element models are shown in Fig. 4 and presented in Table 2. These properties were determined based on experimental data. The concrete was modeled using a fracture-plastic material model (Fig. 4(a)). The fracture-plastic material model in ATENA 3D combines fracture behavior in tension with plastic behavior in compression [25]. In addition to the basic concrete properties presented in Table 2, specific fracture energy, G_F, and crack shear stiffness factor, S_F, were respectively selected as 6.185×10^{-5} MN/m and 20 during model calibration with the experimental data. The anchor rods, connecting the foundation with the column base-plate, were modeled using external cable elements with multilinear stress-strain material as shown in Fig. 5. The elastic modulus of the 19.1 mm diameter anchor rods was set as 189.5 GPa and those of the anchor rods with 25.4 and 31.8 mm

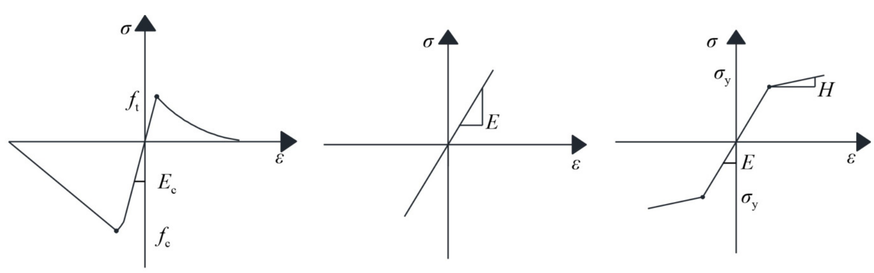

Fig. 4 Material properties: (a) fracture-plastic material model for concrete; (b) linear elastic behavior for steel reinforcement; (c) bilinear stress−strain behavior for structural steel.

Table 2 Material properties assigned to the concrete foundation, steel reinforcement, steel base-plate, and inside and outside flanges

Component	Specimen group	Young's modulus (MPa)	Poisson's ratio	Tensile strength (MPa)	Compressive strength (MPa)	Yield strength (MPa)	Hardening modulus (MPa)
Foundation concrete	S01–S06	31570	0.2	2.5	28.1	–	–
	S07–S10	31570	0.2	2.5	28.1	–	–
Foundation steel reinforcement	S01–S06	200000	–	–	–	–	–
	S07–S10	200000	–	–	–	–	–
Base-plate steel	S01–S06	194000	0.3	–	–	396	2000
	S07–S10	194000	0.3	–	–	396	2000
Inside flange steel	S01–S06	200000	0.3	–	–	423	2000
	S07–S10	194000	0.27	–	–	396	2000
Outside flange steel	S01–S06	200000	0.3	–	–	423	2000
	S07–S10	195600	0.27	–	–	378.5	2000

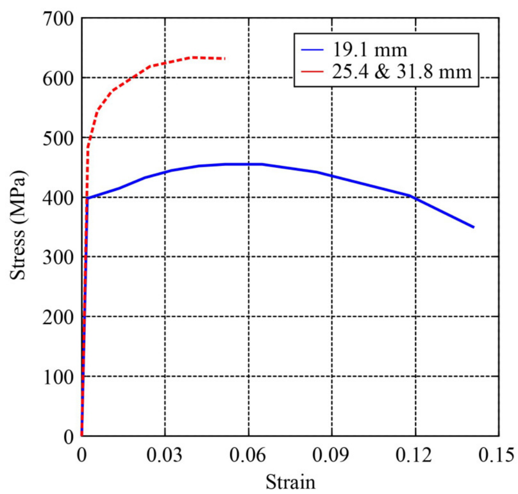

Fig. 5 Measured stress–strain behavior of anchor rods.

diameters were set 211.4 GPa based on experimental data. At one end, the anchor rods were embedded into the base-plate and at the other end they were embedded into the concrete. No agent was used to debond the anchor rods from concrete since this is not the case in the actual construction practice.

The base-plate was modeled using tetrahedral elements (Fig. 3). The top plate of the column connecting the column stub with the transfer beam, as shown in Fig. 3, was modeled using brick elements. The properties of the top plate were the same as those of the base-plate. Additional information regarding the welds and steel plates is provided in Ref. [16]. The beam used for transferring the axial and flexural loads to the specimen was modeled with solid elements having linear elastic properties and an elastic modulus of 200 GPa.

3.4 Finite element mesh and contact interactions

The reinforced concrete foundation was connected to the strong floor by defining a perfect connection between the two macro-elements. The anchor rods were also embedded from the base-plate into the concrete foundation with a perfect connection. The web of the column was perfectly connected to the base-plate, the top plate and the flanges. The top plate was connected to the web and flanges with a perfect connection. The beam used for transferring the axial and flexural loads to the specimen was fully connected with the top plate of the column. The mesh information for the models is provided in Table 3. The final element sizes and the number of elements were determined by trying different meshing options for convergence in conjunction with the selection of the solution parameters presented in Table 4.

Table 3 Mesh information

Element material	Element shape	Element size (mm)	Element type	No. of elements
Concrete foundation	tetrahedral	60	linear	29236
Steel base-plate	tetrahedral	30	quadratic	534
Steel inside flange	brick	75	quadratic	66
Steel outside flange	brick	75	quadratic	66
Steel web	brick	75	quadratic	110
Steel top plate	brick	75	quadratic	18
Steel top beam	brick	150	linear	69
Strong floor	brick	150	linear	64

3.5 Solution method

The analysis was performed using the Newton-Raphson method with line search and tangent stiffness. The line search adjusts the displacement increments to optimize the required work and reduce the out-of-balance forces. The node numbering was optimized using the Sloan algorithm [25] to generate a reduced global stiffness matrix. This algorithm also reduces the memory usage and processor demand for the analysis [25]. Table 4 presents the iteration limit and different error tolerances for the solution method along with the parameters of the line search approach used here.

Table 4 Solution parameters

Method	Parameter	Value
General	iteration limit for one analysis step	100
	displacement error tolerance	0.010000
	residual error tolerance	0.010000
	absolute residual error tolerance	0.010000
	energy error tolerance	0.000100
Line search	unbalanced energy limit	0.800
	limit of line search iterations	2
	line search limit: min.	0.010
	line search limit: max.	1.000

4 Validation of finite element models

The inelastic behavior of the base-plate connections, as presented in Refs. [16–19], was categorized into four damage groups according to their hysteretic behavior and failure mechanisms. The comparison of the experimentally observed and simulated response using the finite element models described above is presented below for each one of the damage groups.

The behavior of 19 mm diameter anchor rods governed the failure of first group of specimens (which included S01 and S02) while slight or no yielding in the flanges, the web and the base-plate was seen. Slight cracking of the reinforced concrete foundation under the base-plate area was also observed. The comparison of S02, which is representative of the first damage group, with the computer simulations is shown in Fig. 6. The behavior of S02 was dominated by a rocking behavior with energy absorption mainly occurring through the yielding of the anchor rods and the ultimate failure due to anchor rod rupture (Figs. 6(a) and 6(b)). This behavior was matched in the finite element models as shown in Fig. 6(a) with slight elastic deformation. Additionally, the von Mises stress contour is shown in Fig. 6(b) where stress concentrations are seen in the first pair of anchor rods in tension. No yielding was seen in the base-plate, web and flanges, which matched the experimental results.

The second damage group included S03 and S04. The failure of the connections in the second damage category was due to combined yielding of the flanges, the base-plate and the web, and moderate cracking of the concrete foundation while the anchor rods were slightly deformed. The condition of S03 after the experiments, which is representative of the second damage group, is shown in Figs. 7(a) and 7(b). Bending of the base-plate was observed, which matched the computer simulations as shown in Fig. 7(a). Additionally, the von Mises stress contours are shown in Fig. 7(b) where stress concentrations were observed in the base-plate and flanges.

The third damage group included S05 and S06. The ultimate failure of S05 and S06 was due to weld rupture between the flanges and the base-plate, while prior to that, yielding of the flanges and the web was observed. The concrete foundation experienced negligible damage and the anchor rods had slight damage. The condition of

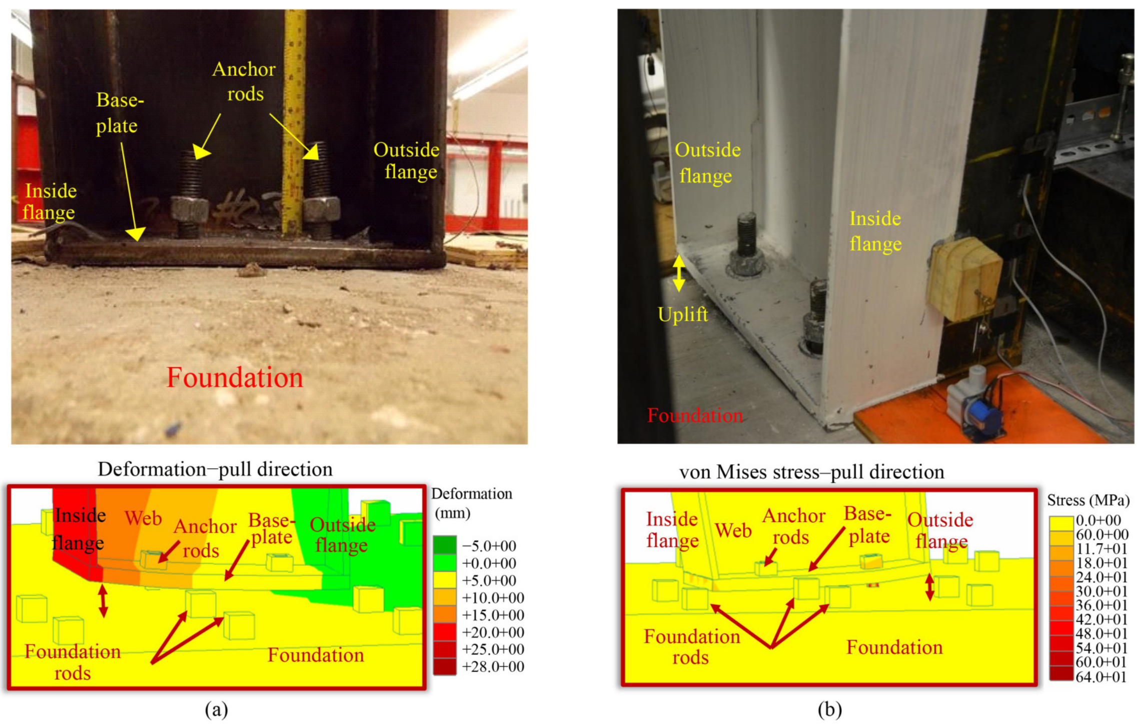

Fig. 6 Typical behavior of the specimens in damage group 1 (images belong to S02): (a) side view with deformations from modeling; (b) oblique view with von Mises stresses from modeling.

S05 after the experiments, which is representative of the third damage group, is shown in Figs. 8(a) and 8(b). A more flexurally dominated behavior of the base-plate was observed, which was matched in the computer models as shown in Fig. 8(a). Additionally, the von Mises stress contours are shown in Fig. 8(b) where yielding was observed in the base-plate, web and flanges. Although the weld rupture was not simulated in the finite element models, von Mises stress contours indicated high stress concentrations between the connections of the base-plate

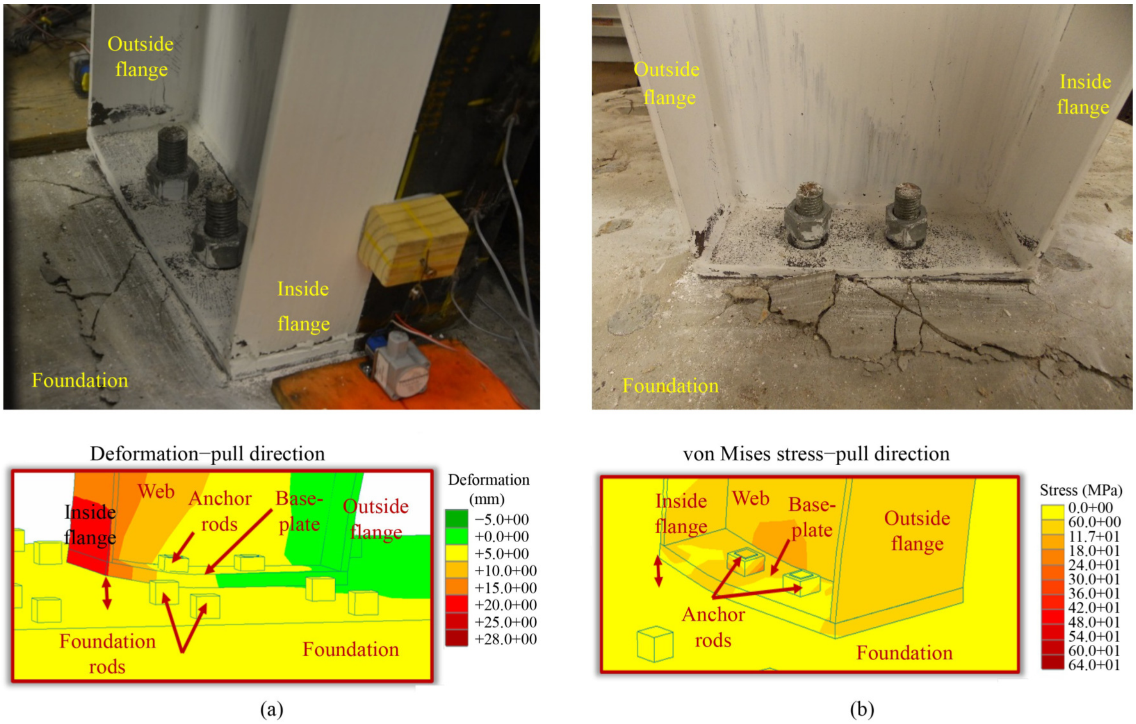

Fig. 7 Typical behavior of the specimens in damage group 2 (images belong to S03): (a) oblique view with deformations from modeling; (b) side view with von Mises stresses from modeling.

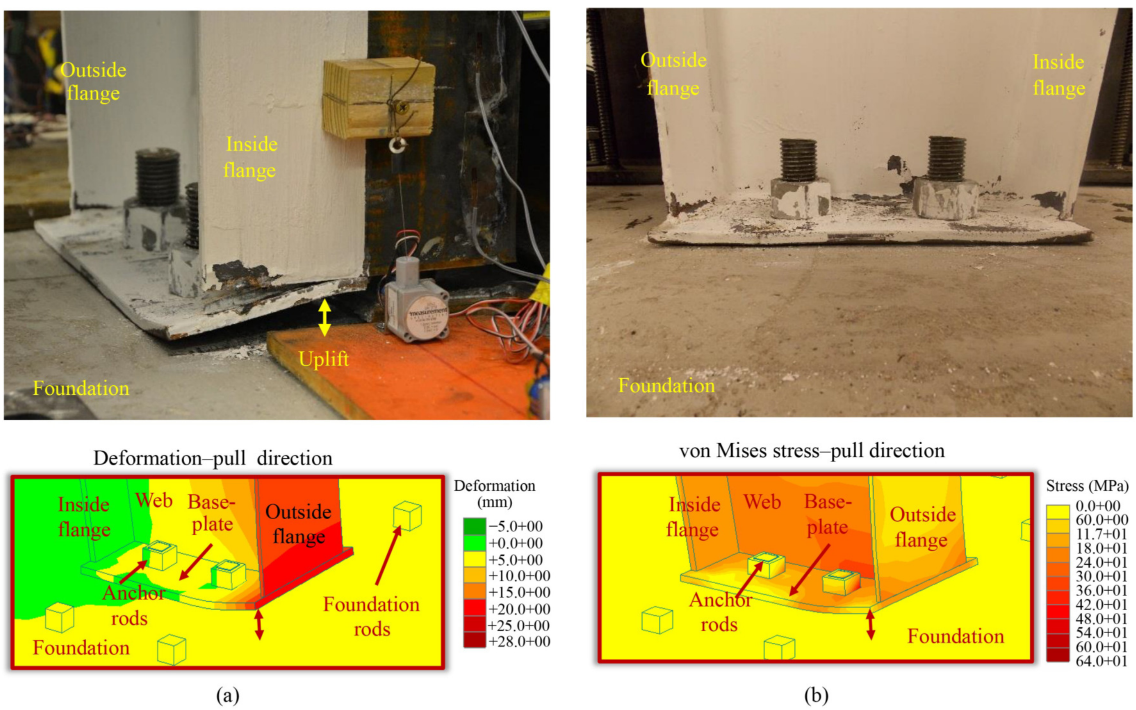

Fig. 8 Typical behavior of the specimens in damage group 3 (images belong to S05): (a) oblique view with deformations from modeling; (b) side view with von Mises stresses from modeling.

with the web and the flanges, capturing the behavior of this group.

The fourth damage group included S07 to S10. The damage of the specimens was governed by the excessive cracking of the concrete foundations and potentially yielding of the reinforcing steel (although this was not measured), and yielding of the base-plate while the flanges, and the anchor rods had slight damage. The condition of S08 after the experiments, which is representative of the fourth damage group, is shown in Figs. 9(a) and 9(b). Excessive cracking of the foundation and bending of the base-plate was observed, which was matched in the computational models as shown in Fig. 9(a). Additionally, the von Mises stress contours shown in Fig. 9(b) indicate that stress concentrations and yielding were observed in the base-plate, web and the flanges. A summary of the damage in the four groups mentioned above are presented in Table 5.

It has been observed from the experimental data presented in Ref. [16] that the envelopes of the cyclic loading closely follow the monotonic loading results. Therefore, a comparison of the monotonic loading results from the computational simulations is made with the envelopes of the cyclic test results from experiments in Ref. [16]. Figures 10 and 11 show a comparison of the moment–rotation responses obtained from finite element models with those from experiments for the first and second groups of specimens, respectively. A comparison of the average moment capacity and average rotational stiffness of the connections obtained from the push and pull directions of the computational analysis and the experiments are summarized in Figs. 12(a) and 12(b), respectively. The moment was obtained by multiplying the lateral force by the height measured from the column base to the top where the load was applied. The rotation was measured as the difference in the upward displacements of the two column flanges divided by the distance between the flanges. The elastic (secant) rotational stiffness of the connections from the computational models was calculated at the 0.75% drift limit. The numbers above the charts indicate the difference of the model results with respect to the experiments. It was observed that the moment capacities of the base-plate connections estimated with the finite

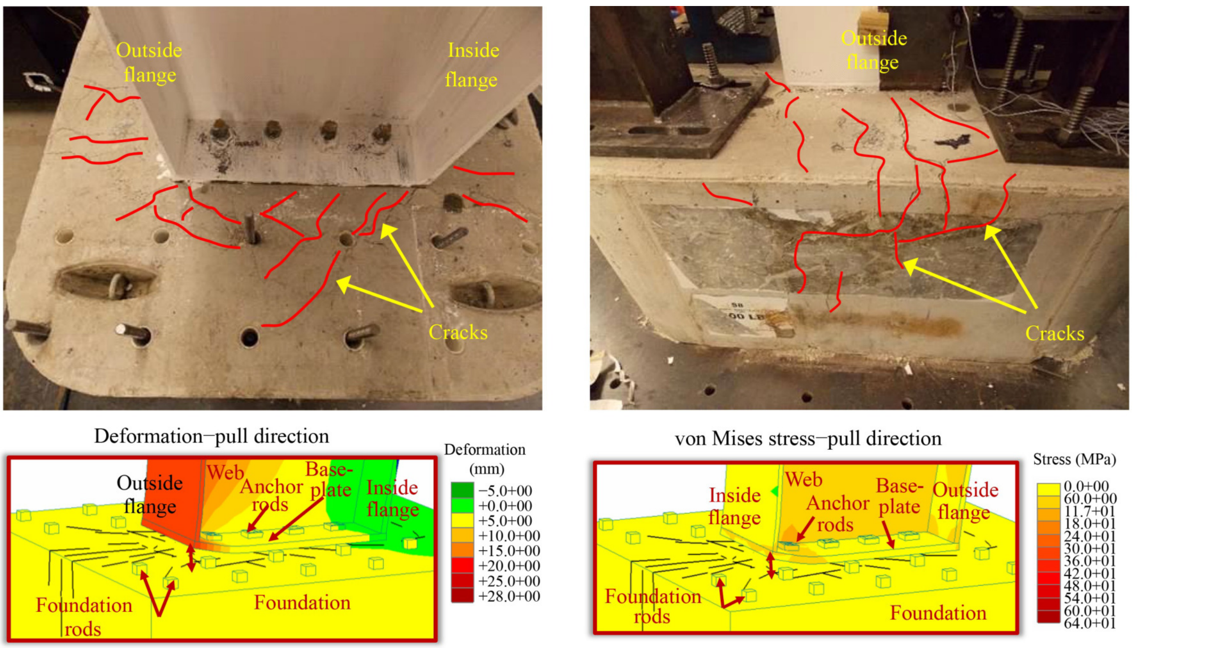

(a) (b)

Fig. 9 Typical behavior of the specimens in damage group 4 (images belong to S08): (a) side view with deformations from modeling; (b) back view with von Mises stresses from modeling.

Table 5 Summary of the failure modes in the experiments and simulations

Damage group	Experiment	Simulation
S01 and S02	yielding and rupture of anchor rods	yielding and rupture of anchor rods
S03 and S04	combined yielding of flanges and web as well as yielding and bending of base-plate, and moderate cracking of concrete foundation	combined yielding of flanges and web as well as yielding and bending of base-plate
S05 and S06	yielding of flanges and web as well as yielding and bending of base-plate and weld rupture between flanges and base-plate	yielding of flanges and web as well as yielding and bending of base-plate and high stress concentration between connections of base-plate with flanges and web
S07 to S10	excessive cracking of concrete foundation and yielding of base-plate	excessive cracking of concrete foundation and yielding of and bending of base-plate as well as yielding of flanges and web

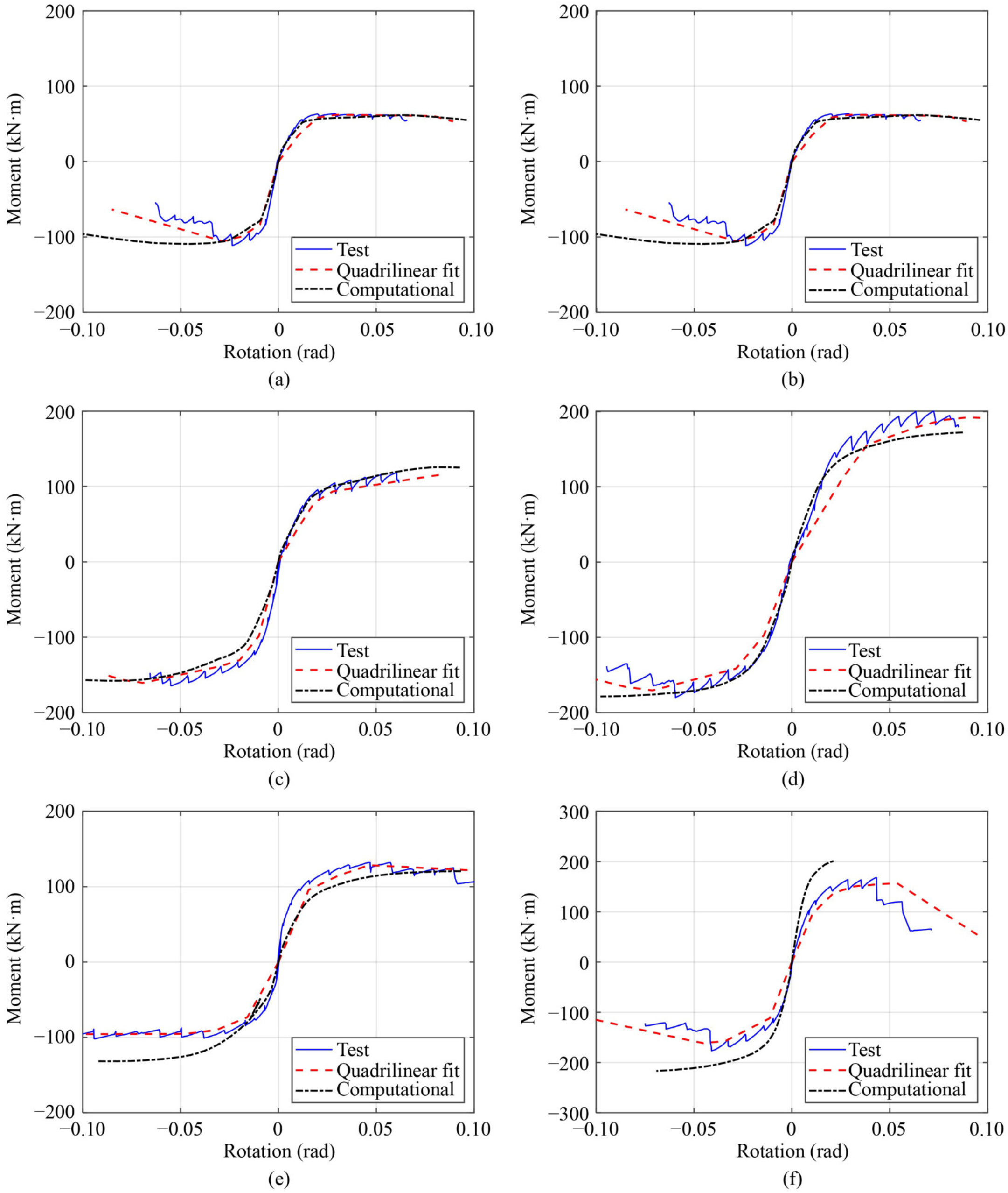

Fig. 10 Comparison of the experimental (blue), quadrilinear fitted curve to experiments (red) and computational (black) moment–rotation responses for first group of specimens: (a) S01; (b) S02; (c) S03; (d) S04; (e) S05; (f) S06.

element models are in a good agreement with the ones calculated from the experimental results. The average rotational stiffnesses obtained from the 3D finite element models differed from the experimental results by 15% to 61%. The average moment capacities, on the other hand, differed only by up to 24%. It is noted that there is a larger discrepancy between the rotational stiffnesses obtained from the computational models and the experiments. Given the high sensitivity of the rotation measurements that need to be recorded at small displacements in experiments, these results were found reasonable, and adequate for a comparative parametric study between different column base-plate configurations, which is the main purpose of this research.

5 Parametric study

The validated 3D finite element models were utilized for a parametric investigation under the same axial load to understand the effect of the connection design variables on the rotational stiffness and moment capacity. The authors worked with the Metal Building Manufacturer's Association (MBMA) in the United States to select the base-plate connection configurations for the parametric study based on the most commonly used designs. Two

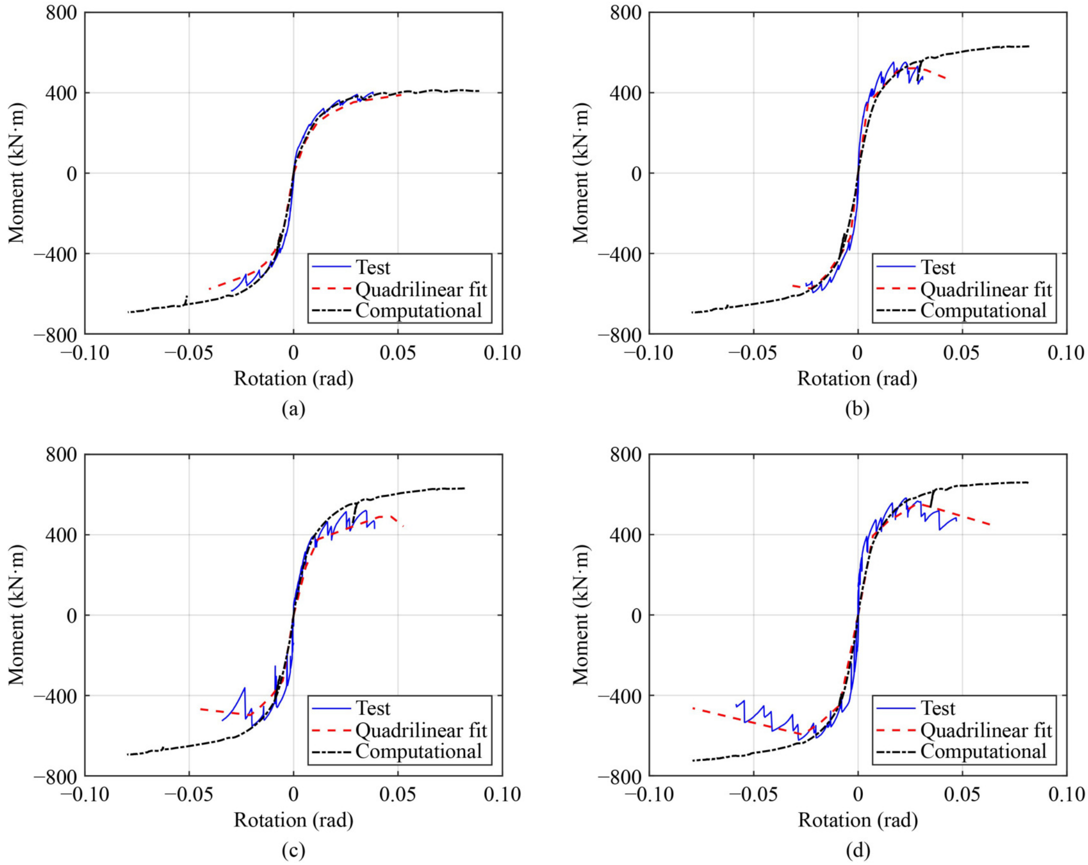

Fig. 11 Comparison of the experimental (blue), quadrilinear fitted curve to experiments (red) and computational (black) moment–rotation responses for second group of specimens: (a) S07; (b) S08; (c) S09; (d) S10.

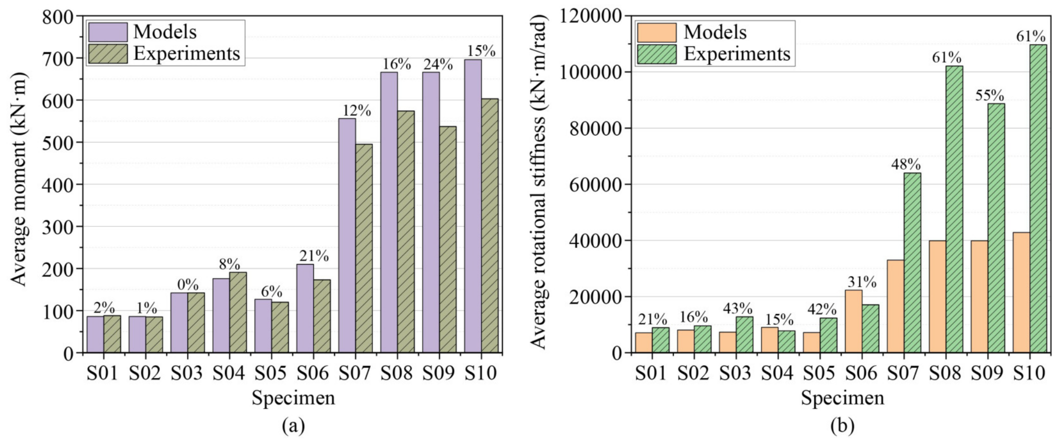

Fig. 12 Comparison of (a) average moment; (b) average rotational stiffness between the computational models and the experimental results.

column base-plate connections with web-depths of 305 and 558 mm were chosen as representatives of real base-plate connections in low-rise buildings. Twenty-nine and thirty different column base-plate connection combinations were created for the 305 and 558 mm web depths, respectively. The base-plate connection models are shown in Fig. 13 and the model combinations for the 305 and the 558 mm web depth connections are presented in Table 6 (refer to Fig. 2 for geometric characteristics). In Table 6, the parameters for the base (i.e., reference) model connections, P01 and P02, are presented in addition to the parameters that are only changed from the reference configurations (P01 or P02) for each of the parametric cases. The parameters under investigation were the flange width, web thickness, flanges thicknesses, base-plate width, base-plate thickness, anchor rod diameter, combination of base-plate thickness and anchor rod diameter, number of anchor rods, and the pitch,

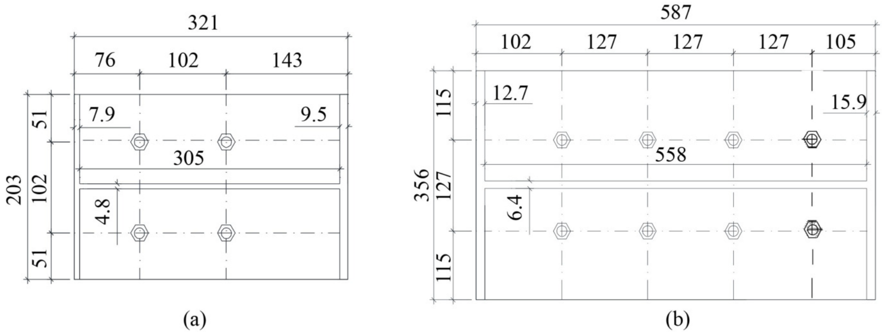

Fig. 13 Column base-plate connections for (a) 305 mm web depth connections (P01) and (b) 558 mm web depth connections (P02).

Table 6 Parametric analysis matrix for the 305 and 558 mm web depth, d_w, column base-plate connections

P01 parametric model ID	Parameter and value for P01 reference model (d_w = 305 mm)	Value for P01 parametric models (mm)	P02 parametric model ID	Parameter and value for P02 reference model (d_w = 558 mm)	Value for P02 parametric models (mm)
P01-01	flange width b_f (P01 = 203 mm)	152	P02-01	flange width b_f (P02 = 356 mm)	254
P01-02		254	P02-02		305
P01-03		305	P02-03		407
P01-04	web thickness t_w (P01 = 4.8 mm)	6.4	P02-04	web thickness t_w (P02 = 6.4 mm)	4.8
P01-05		8.0	P02-05		7.9
P01-06		11.2	P02-06		11.1
P01-07	flanges thicknesses t_{fo} (P01 = 7.9 mm) and t_{fi} (P01 = 9.5 mm)	6.3 and 7.9	P02-07	flanges thicknesses t_{fo} (P02 = 12.7 mm) and t_{fi} (P02 = 15.9 mm)	11.1 and 8.0
P01-08		9.5 and 11.1	P02-08		14.3 and 17.5
P01-09		11.1 and 9.5	P02-09		15.9 and 19.1
P01-10		12.6 and 11.1	P02-10		12.7 and 12.7
P01-11	base-plate width b_{bp} (P01 = 203 mm)	254	P02-11	base-plate width b_{bp} (P02 = 356 mm)	406
P01-12		305	P02-12		457
P01-13		356	P02-13		508
P01-14	base-plate thickness t_p (P01 = 15.9 mm)	19.1	P02-14	base-plate thickness t_p (P02 = 15.9 mm)	9.5
P01-15		22.2	P02-15		12.7
P01-16		25.4	P02-16		19.1
P01-17	anchor rod diameter d_b (P01 = 19.1 mm)	25.4	P02-17	anchor rod diameter d_b (P02 = 31.8 mm)	19.1
P01-18		31.8	P02-18		25.4
P01-19	base-plate thickness t_p (P01 = 15.9 mm) and anchor rod diameter d_b (P01 = 19.1 mm)	19.1 and 25.4	P02-19	base-plate thickness t_p (P02 = 15.9 mm) and anchor rod diameter d_b (P02 = 31.8 mm)	9.5 and 19.1
P01-20		22.2 and 25.4	P02-20		12.7 and 19.1
P01-21		25.4 and 25.4	P02-21		19.1 and 19.1
P01-22		19.1 and 31.8	P02-22		9.5 and 25.4
P01-23		22.2 and 31.8	P02-23		12.7 and 25.4
P01-24		25.4 and 31.8	P02-24		19.1 and 25.4
P01-25	number of anchor rods (P01 = 4)	6	P02-25	number of anchor rods (P02 = 8)	6
P01-26	pitch S_1 (P01 = 102 mm)	127	P02-26	pitch S_1 (P02 = 127 mm)	152
P01-27		152	P02-27	setback S_0 (P02 = 102 mm)	127
P01-28	setback S_0 (P01 = 76 mm)	102	P02-28		152
P01-29		127	P02-29	gage g (P02 = 127 mm)	152
–	–	–	P02-30		203

setback and gage distances of the anchor rods. It should be noted that the minimum requirements for the 25.4 mm anchor rod diameter are 102 mm setback and 254 mm base-plate width, and those for the 31.75 mm anchor rod diameter are 102 mm setback, 127 mm pitch, 127 mm gage and 254 mm base-plate width. These requirements were followed in selecting the variations of the parameters.

The lateral and rotational stiffnesses and the moment capacities of the reference connection configurations, i.e., P01 and P02, and comparisons with the parametrized configurations are summarized in Figs. 14–17 for the push and pull directions. The rotational stiffnesses presented in the parametric analyses were calculated at the 0.75% drift.

Figures 14 and 15 present the results for P01 models

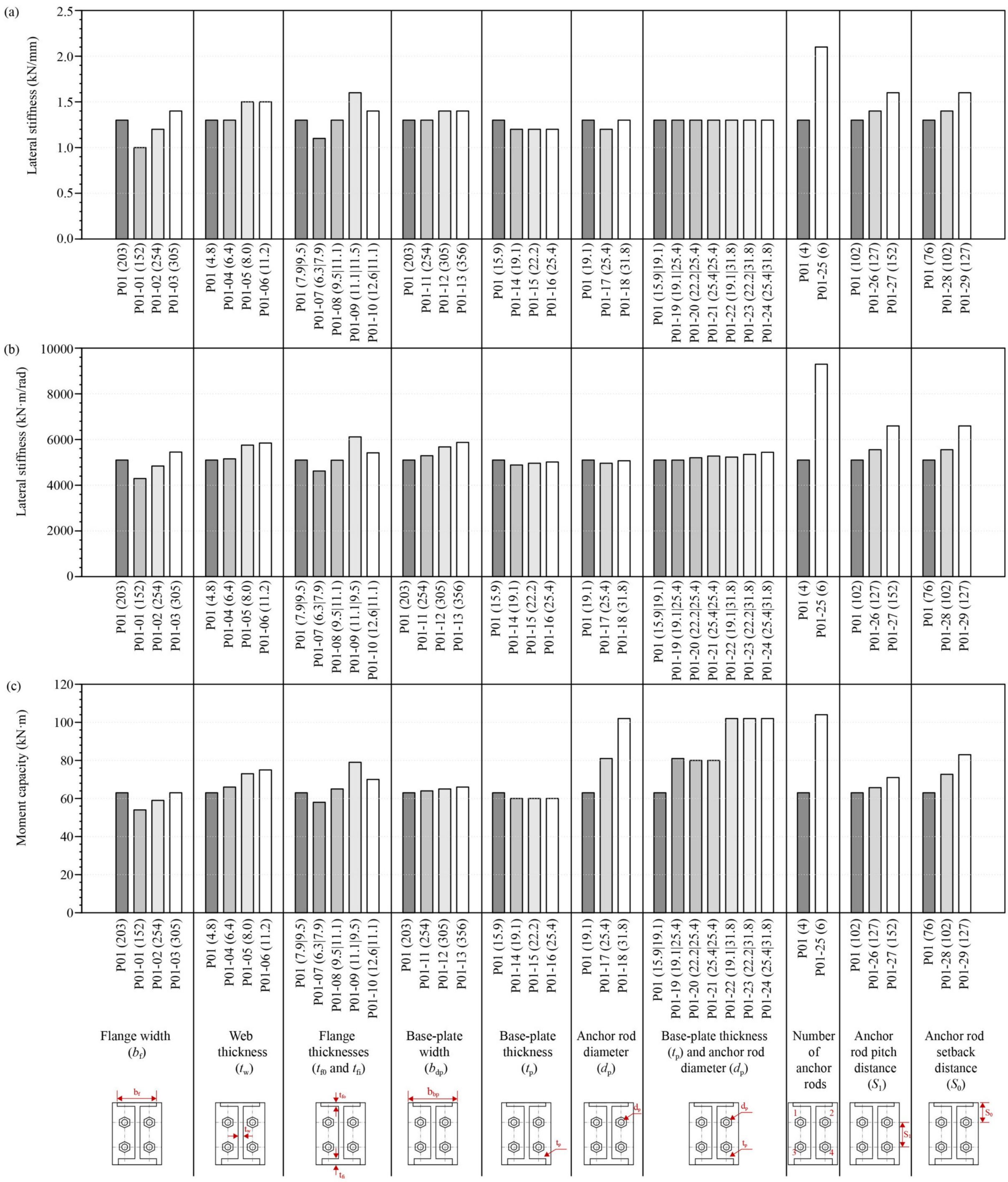

Fig. 14 Results of parametric analysis in push direction for 305 mm, P01, web depth column base-plate connections: (a) lateral stiffness; (b) rotational stiffness; (c) moment capacity.

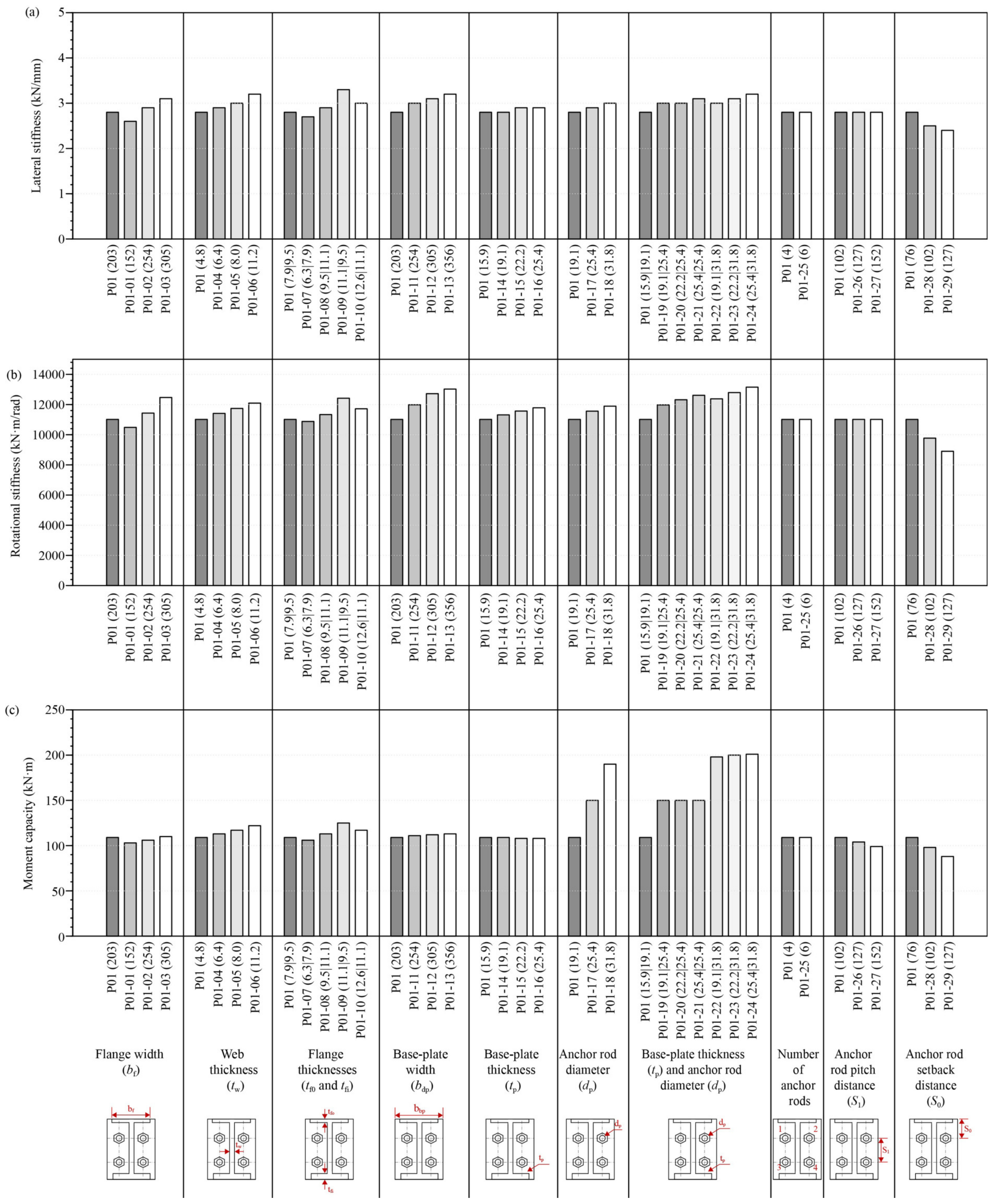

Fig. 15 Results of parametric analysis in pull direction for 305 mm, P01, web depth column base-plate connections: (a) lateral stiffness; (b) rotational stiffness; (c) moment capacity.

with the 305 mm web depth. Based on the results of P01 and P01-01 to P01-03, it is seen that the use of a lager flange width resulted in a higher lateral and rotational stiffnesses for P01 models but did not change the moment capacity. Increasing the flange width by 102 mm, or 50%, resulted in a higher lateral and rotational stiffnesses by 8% and 7%, respectively, in the push direction and by 11% and 13%, respectively, in the pull direction. On the other hand, reducing the flange width by 51 mm, or 25%, resulted in lower lateral and rotational stiffnesses and moment capacity by 23%, 16%, and 14%, respectively, in the push direction and by 7%, 5%, and 6%, respectively, in the pull direction.

Based on the results of P01 and P01-04 to P01-06,

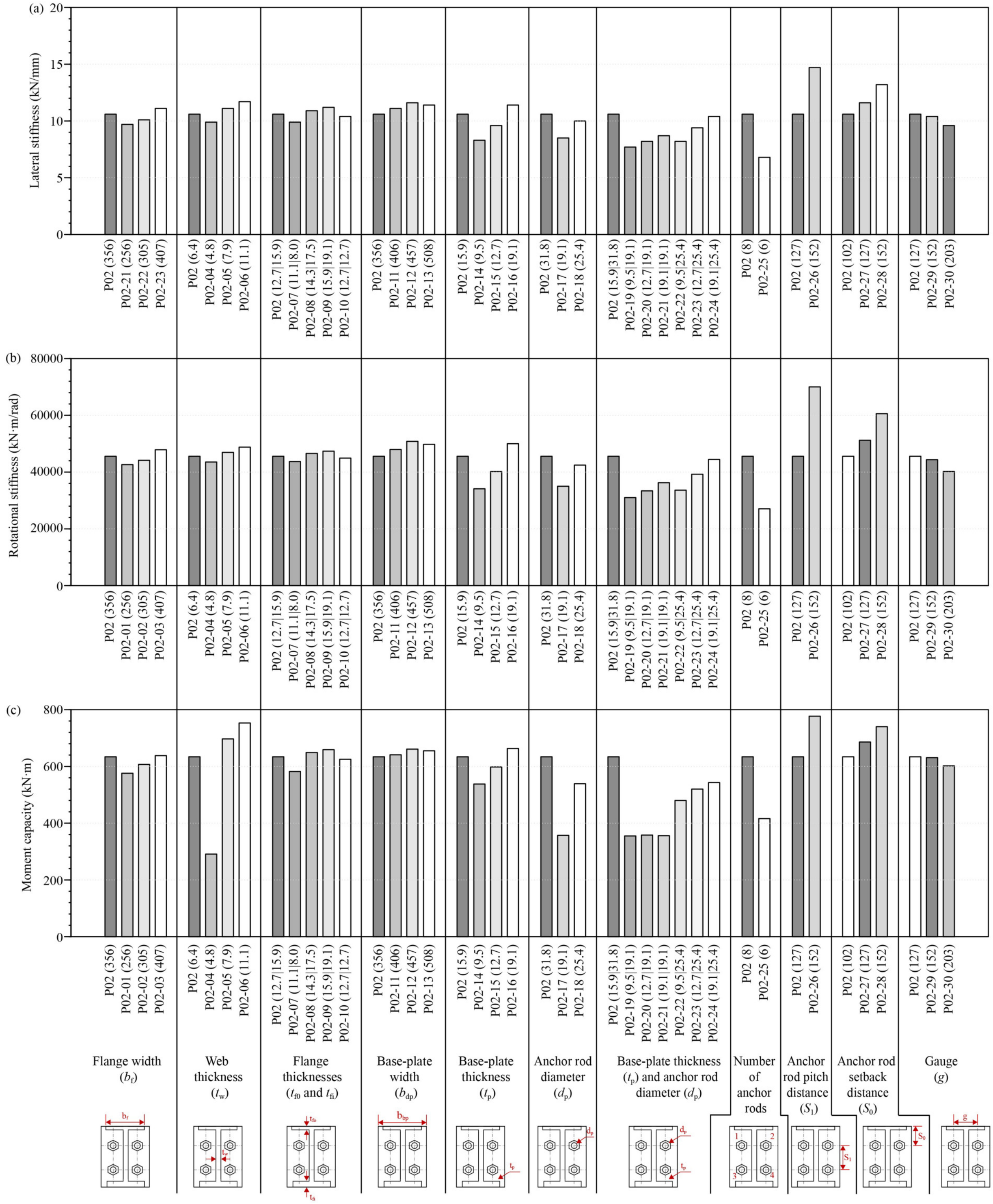

Fig. 16 Results of parametric analysis in push direction for 558 mm, P02, web depth column base-plate connections: (a) lateral stiffness; (b) rotational stiffness; (c) moment capacity.

increasing the web thickness by 6.4 mm, or 133%, resulted in higher lateral and rotational stiffnesses and moment capacity by 15%, 15%, and 19%, respectively, in the push direction and by 14%, 10%, and 12%, respectively, in the pull direction.

Based on the results of P01 and P01-07 to P01-10, increasing the inside and outside flange thicknesses by 1.6 mm, or 17%, and 4.7 mm, or 59%, respectively, resulted in higher lateral and rotational stiffnesses and moment capacity by 8%, 6%, and 11%, respectively, in the push direction and 7%, 6%, and 7%, respectively, in the pull direction. On the other hand, reducing the inside and outside flange thicknesses by 1.6 mm, or 17%, and 1.6 mm, or 20%, resulted in lower lateral and rotational

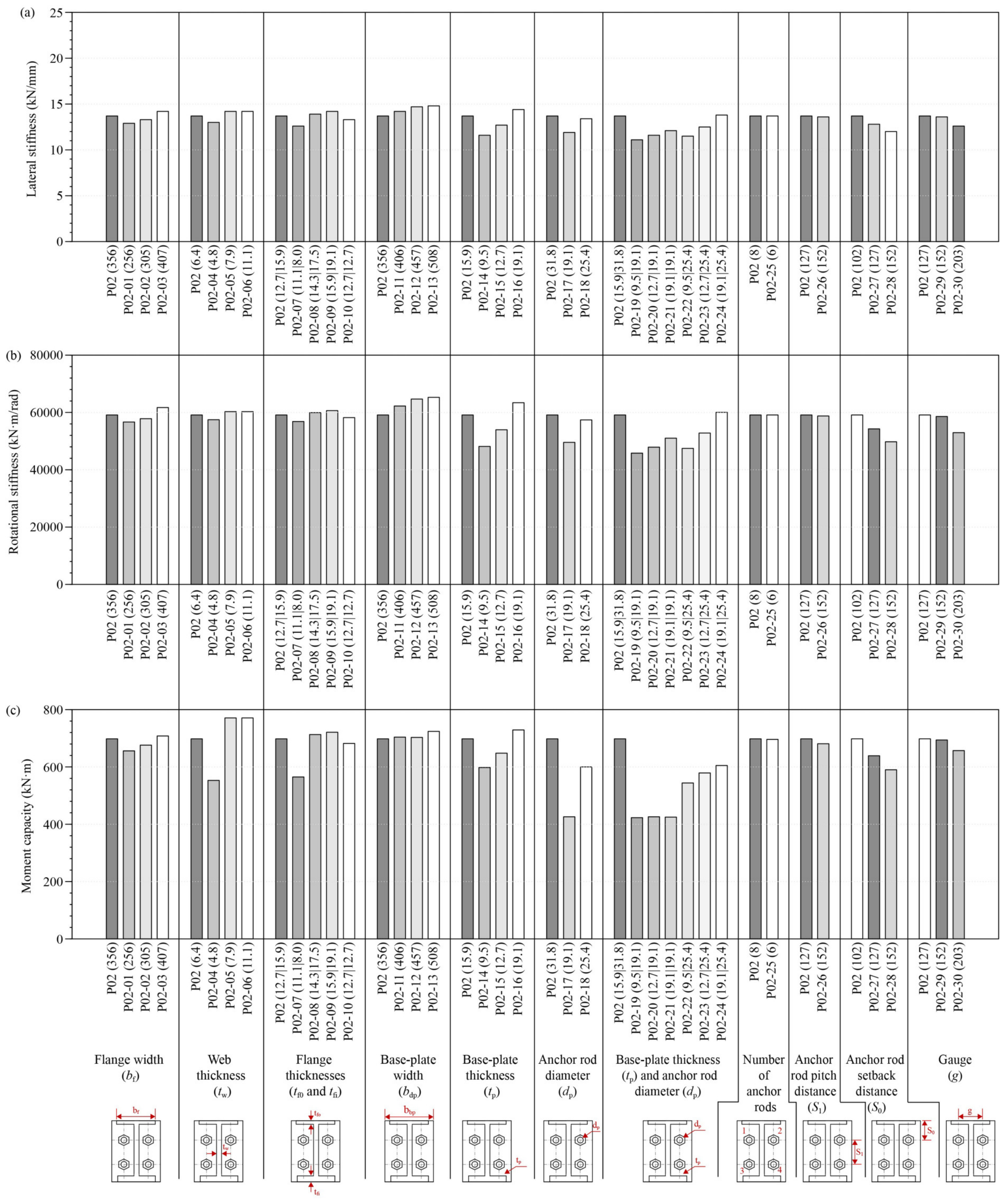

Fig. 17 Results of parametric analysis in pull direction for 558 mm, P02, web depth column base-plate connections: (a) lateral stiffness; (b) rotational stiffness; (c) moment capacity.

stiffnesses and moment capacity by 15%, 9%, and 8%, respectively, in the push direction, and 4%, 1%, and 3%, respectively, in the pull direction.

Based on the results of P01 and P01-11 to P01-13, increasing the base-plate width by 153 mm, or 75%, resulted in higher lateral and rotational stiffnesses and moment capacity by 8%, 15%, and 5%, respectively, in the push direction and by 14%, 18%, and 4%, respectively, in the pull direction.

Based on the results of P01 and P01-14 to P01-16, increasing the base-plate thickness by 9.5 mm, or 60%, increased the lateral and rotational stiffnesses in the pull direction by 4% and 7%, respectively, but did not improve these properties in the push direction nor the moment capacity in either direction.

Based on the results of P01 and P01-17 and P01-18, increasing the anchor rod diameter by 12.7 mm, or 66%, increased the moment capacity in the push and pull directions by 62% and 74%, respectively. It is also noted when the anchor rod diameter was increased by 6.3 mm, or 33%, the increase in the moment capacity in the push and pull directions was 29% and 38%, respectively. In terms of stiffness, a 66% increase in the anchor rod diameter increased the lateral and rotational stiffnesses only in the pull direction by 7% and 8%, respectively.

Based on the results of P01 and P01-19 to P01-21, increasing the base-plate thickness by 9.5 mm, or 60%, at the same time with the anchor rod diameter by 6.3 mm, or 33%, resulted in higher lateral and rotational stiffnesses and moment capacity of 0% (i.e., no change), 3%, and 27%, respectively, in the push direction and by 11%, 14%, and 38%, respectively, in the pull direction. The same increase in the base-plate thickness, 9.5 mm, or 60%, but along with a larger increase of the anchor rod diameter by 12.7 mm, or 66%, i.e., models P01-22 to P01-24, resulted in higher linear and rotational stiffnesses and moment capacity by 0% (i.e., no change), 7%, and 62%, respectively, in the push direction and by 14%, 19%, and 84%, respectively, in the pull direction compared to the reference model, P01.

Based on the results of P01 and P01-25 models, increasing the number of anchor rods from four to six increased the lateral and rotational stiffnesses and moment capacity by 62%, 82%, and 65%, respectively, in the push direction but no change was observed in the pull direction.

Based on the results of P01 and P01-26 and P01-27, increasing the anchor rod pitch by 50 mm, or 49%, resulted in higher lateral and rotational stiffnesses and moment capacity by 23%, 29%, and 13%, respectively, in the push direction but in the pull direction no increase was observed in terms of stiffnesses, and the moment capacity reduced by 9%.

Based on the results of P01 and P01-28 and P01-29, increasing the anchor rod setback by 51 mm, or 67%, increased the lateral and rotational stiffnesses and moment capacity by 23%, 29%, and 32%, respectively, in the push direction but caused these properties to decline in the pull direction by 14%, 19%, and 19%, respectively.

Based on these results, the anchor rod diameter, by itself or in combination with the base-plate thickness, was found to be the most influential variable on the moment capacity of the P01 models as shown in Figs. 18 and 19 in terms of moment versus rotation and load versus deformation curves, respectively. The number of anchor rods was also influential on the lateral and rotational stiffnesses and moment capacity but only in the push direction. In terms of lateral and rotational stiffnesses of P01 models, the number of anchor rods as well as the anchor rod pitch and setback were the most influential variables specifically in the push direction.

Figures 16 and 17 present the results for P02 models with 558 mm web depth details of which are shown in Table 6. Based on the results of P02 and P02-1 to P02-3, it is seen that increasing the flange width by 51 mm, or 14%, resulted in 5% and 4% higher lateral and rotational stiffnesses in the push and pull directions, respectively, but no change in the moment capacity was observed in either direction. On the other hand, decreasing the flange width by 102 mm, or 29%, reduced the lateral and rotational stiffnesses and moment capacity by 8%, 6%, and 9%, respectively, in the push direction and by 6%, 4%, and 6%, respectively, in the pull direction.

Based on the results of P02 and P02-04 to P02-06, increasing the web thickness by 4.7 mm, or 73%, increased the lateral and rotational stiffnesses and

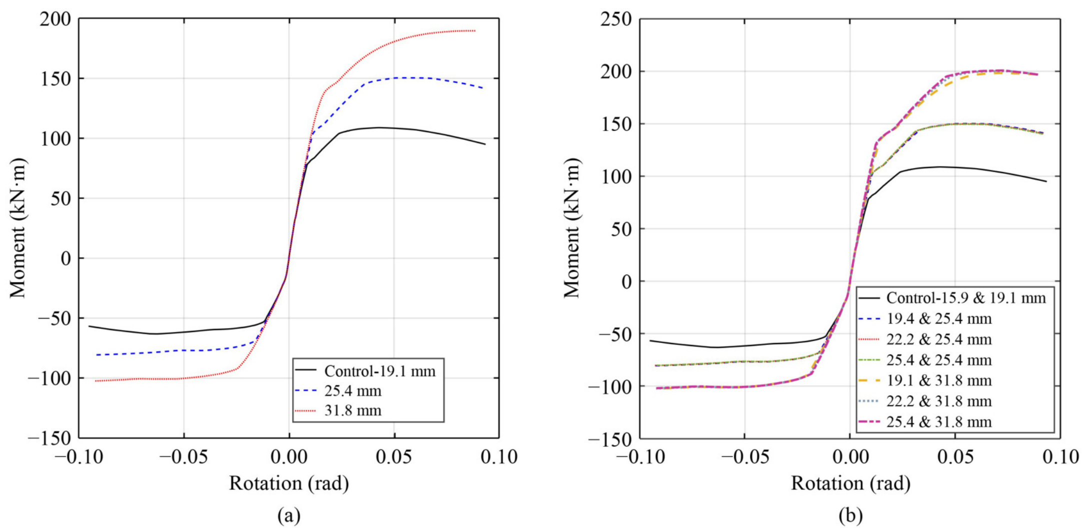

Fig. 18 Moment–rotation behavior of base-plate connections with 305 mm web depth and different parameters: (a) anchor rod diameter; (b) combined base-plate thickness and anchor rod diameter.

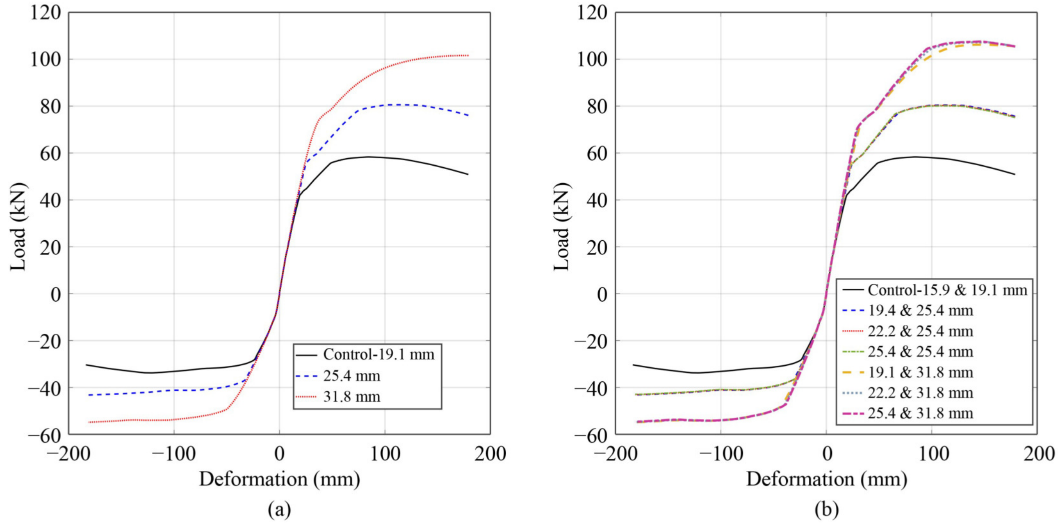

Fig. 19 Load–deformation behavior of base-plate connections with 305 mm web depth and different parameters: (a) anchor rod diameter; (b) combined base-plate thickness and anchor rod diameter.

moment capacity by 10%, 7%, and 19%, respectively, in the push direction and by 4%, 0% (i.e., no change), and 10%, respectively, in the pull direction. On the other hand, reducing the web thickness by 1.6 mm, or 25%, reduced the lateral and rotational stiffnesses and moment capacity by 7%, 4%, and 54%, respectively, in the push direction and by 5%, 3%, and 21%, respectively, in the pull direction.

Based on the results of P02 and P02-07 to P02-10, reducing the inside and outside flange thicknesses by 7.9 mm, or 50%, and 1.6 mm, or 13%, decreased the lateral and rotational stiffnesses and moment capacity by 7%, 4%, and 8%, respectively, in the push direction and 8%, 4%, and 19%, respectively, in the pull direction. On the other hand, increasing the inside and outside flange thicknesses by 3.2 mm, or 20%, and 3.2 mm, or 25% increased the lateral and rotational stiffnesses and moment capacity by 6%, 4%, and 4%, respectively, in the push direction and by 4%, 3%, and 3%, respectively, in the pull direction. Additionally, keeping the outside flange thickness the same and reducing the inside flange thickness by 3.2 mm, or 20%, decreased the lateral and rotational stiffnesses and moment capacity negligibly by 2%, 1%, and 1%, respectively, in the push direction and by 4%, 2%, and 2%, respectively, in the pull direction.

Based on the results of P02 and P02-11 to P02-13, increasing the base-plate width by 152 mm, or 43%, increased the lateral and rotational stiffnesses and moment capacity by 8%, 9%, and 3%, respectively, in the push direction and by 8%, 10%, and 4%, respectively, in the pull direction.

Based on the results of P02 and P02-14 to P02-16, increasing the base-plate thickness by 3.2 mm, or 20%, increased the lateral and rotational stiffnesses and moment capacity by 8%, 10%, and 5%, respectively, in the push direction and by 5%, 7%, and 4%, respectively, in the pull direction. On the other hand, decreasing the base-plate thickness by 6.4 mm, or 40%, reduced the lateral and rotational stiffnesses and moment capacity by 22%, 25%, and 15%, respectively, in the push direction and by 15%, 19%, and 14%, respectively, in the pull direction.

Based on the results of P02 and P02-17 and P02-18, decreasing the anchor rod diameter by 12.7 mm, or 40%, reduced the lateral and rotational stiffnesses and moment capacity by 20%, 23%, and 44%, respectively, in the push direction and by 13%, 16%, and 39%, respectively, in the pull direction.

Based on the results of P02 and P02-19 to P02-24, decreasing the anchor rod diameter by 12.7 mm, or 40%, and at the same time reducing the base-plate thickness by 6.4 mm, or 40%, caused the lateral and rotational stiffnesses and moment capacity to reduce by 27%, 32%, and 44%, respectively, in the push direction and by 19%, 23%, and 39%, respectively, in the pull direction . On the other hand, decreasing the anchor rod diameter by the same amount, 12.7 mm, or 40%, but increasing the base-plate thickness by 3.2 mm, or 20%, limited the reduction in lateral and rotational stiffnesses and moment capacity to 18%, 20%, and 44%, respectively, in the push direction and to 12%, 14%, and 39%, respectively, in the pull direction compared to the reference model, i.e., P02. It was also shown that decreasing the anchor rod diameter by 6.4 mm, or 20%, rather than 40%, and increasing the base-plate thickness by 3.2 mm, or 20%, yielded similar lateral and rotational stiffnesses and moment capacity to the reference model.

Based on the results of P02 and P02-25, decreasing the number of anchor rods from eight to six reduced the lateral and rotational stiffnesses and moment capacity in the push direction by 36%, 41%, and 34%, respectively, but did not change these properties in the pull direction.

Based on the results of P02 and P02-26, increasing the anchor rod pitch by 25 mm, or 20%, increased the lateral and rotational stiffnesses and moment capacity in the push direction by 39%, 54%, and 23%, respectively, but did not change the stiffness parameters in the pull direction and only reduced the moment capacity in the pull direction by 2%.

Based on the results of P02 and P02-27 and P02-28, increasing the anchor rod setback by 50 mm, or 49%, raised the lateral and rotational stiffnesses and moment capacity in the push direction by 25%, 33%, and 17%, respectively, but reduced these parameters in the pull direction by 12%, 16%, and 15%, respectively.

Based on the results of P02 and P02-29 and P02-30, increasing the anchor rod gage by 25 mm, or 20%, did not affect the stiffnesses and moment capacity in the push and pull directions but increasing the gage by 76 mm, or 60%, reduced the lateral and rotational stiffnesses and moment capacity by 9%, 12%, and 5%, respectively, in the push direction and 8%, 10%, and 6%, respectively, in the pull direction.

Based on these results, anchor rod diameter, by itself or in combination with base-plate thickness, was found to be the most influential variable on the lateral and rotational stiffness and moment capacity of P02 models both in the pull and push directions as shown in Figs. 20 and 21 in terms of moment versus rotation and load versus deformation, respectively. The number of anchor rods also influenced the lateral and rotational stiffnesses and moment capacity but only in the push direction. Base-plate thickness, anchor rod pitch and setback were influential on the lateral and rotational stiffnesses of the

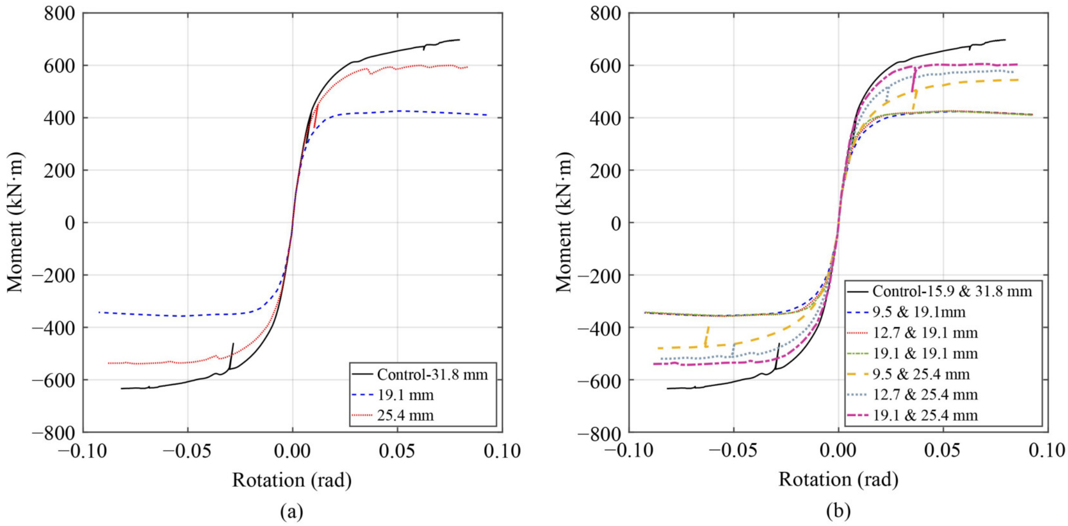

Fig. 20 Moment–rotation behavior of base-plate connections with 558 mm web depth and different parameters: (a) anchor rod diameter; (b) combined base-plate thickness and anchor rod diameter.

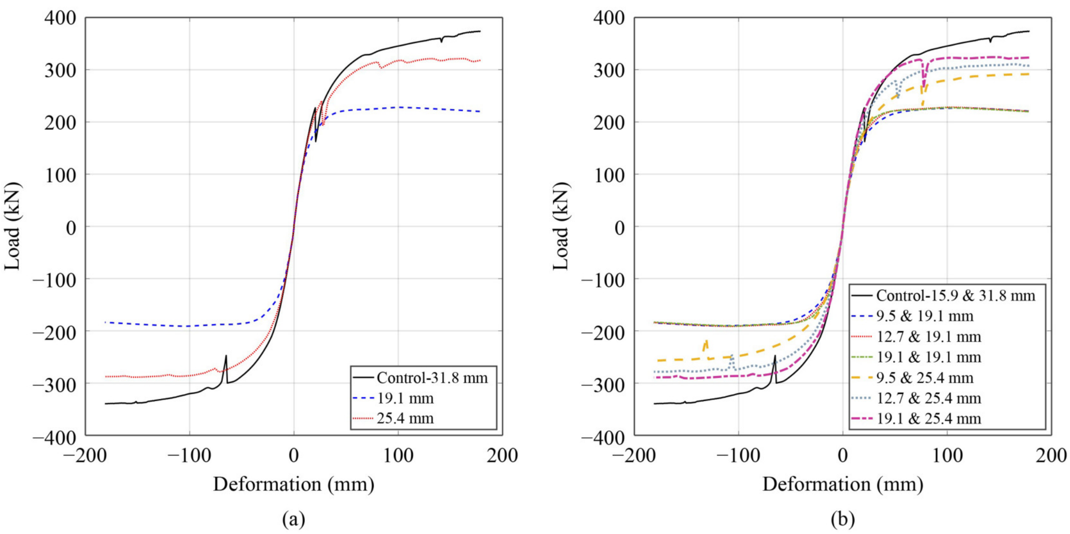

Fig. 21 Load–deformation behavior of base-plate connections with 558 mm web depth and different parameters: (a) anchor rod diameter; (b) combined base-plate thickness and anchor rod diameter.

P02 models especially in the push direction. Web thickness was also influential on the moment capacity of the P02 models.

6 Conclusions

In this paper, a computational approach was undertaken to evaluate pinned column base-plate connections and identify the most influential variables on their behavior under combined axial and lateral loading. First, computational models were developed and validated using previously conducted experiments. The validated models were then used to perform a parametric study to assess the influence of different variables on the lateral and rotational stiffnesses and moment capacity of the connection models with 305 mm web depth, P01, and 558 mm web depth, P02. The investigated variables included the flange width, web thickness, inside and outside flanges thicknesses, base-plate width, base-plate thickness, anchor rod diameter, combination of anchor rod diameter and base-plate thickness, number of anchor rods, and anchor rod pitch, setback, and gage. The main findings are summarized below.

1) Anchor rod diameter, by itself and in combination with base-plate thickness, was found to be the most influential parameter on the moment capacity of P01 models. An increase of 12.7 mm, or 66%, in the diameter of the anchor rods resulted in 62% and 74% increase in the moment capacity of P01 models in the push and pull directions, respectively. Among other parameters, the anchor rod diameter also had the highest impact on the lateral and rotational stiffnesses and moment capacity of P02 models. Decreasing the anchor rod diameter by 12.7 mm, or 40%, at the same time with reducing the base-plate thickness by 6.4 mm, or 40%, caused the lateral and rotational stiffnesses and moment capacity of P02 model to reduce by 27%, 32%, and 44%, respectively, in the push direction and by 19%, 23%, and 39%, respectively, in the pull direction.

2) The number of anchor rods showed the highest influence on the lateral and rotational stiffnesses and moment capacity of P01 and P02 models only in the push direction. Increasing the number of anchor rods from four to six increased the lateral and rotational stiffnesses and moment capacity of P01 models by 62%, 82%, and 65%, respectively, in the push direction. Decreasing the number of anchor rods from eight to six reduced the lateral and rotational stiffnesses and moment capacity of P02 models by 36%, 41%, and 34%, respectively, in the push direction.

3) The anchor rod pitch and setback were found to be influential on the lateral and rotational stiffnesses of P01 and P02 models especially in the push direction. In the case of P02 models, increasing the pitch by 25 mm, or 20%, increased the lateral and rotational stiffnesses in the push direction by 39% and 54%, respectively. Additionally, increasing the setback by 50 mm, or 49%, increased the lateral and rotational stiffnesses in the push direction by 25% and 33%, respectively.

4) Decreasing the web thickness of P02 model by 1.6 mm, or 25%, reduced the moment capacity of the model by 54% and 21% in the push and pull directions, respectively.

Acknowledgements The authors are thankful to Dr. Xiaoying Pan for her assistance in some of the data processing.

Funding note Open access funding provided by SCELC, Statewide California Electronic Library Consortium.

Competing interests The authors declare that they have no competing interests.

References

1. Targowski R, Lamblin D, Guerlement G. Base plate column connection under bending: Experimental and numerical study. Journal of Constructional Steel Research, 1993, 27: 37–54
2. Thambiratnam D P, Krishnamurthy N. Computer analysis of column base plates. Computers & Structures, 1989, 33(3): 839–850
3. Kontoleon M J, Mistakidis E S, Baniotopoulos C C, Panagiotopoulos P D. Parametric analysis of the structural response of steel base plate connections. Computers & Structures, 1999, 71(1): 87–103
4. Dumas M, Beaulieu D, Picard A. Characterization equations for steel column base connections. Canadian Journal of Civil Engineering, 2006, 33(4): 409–420
5. Hamizi M, Hannachi N E. Evaluation by a finite element method of the flexibility factor and fixity degree for the base plate connections commonly used. Strength of Materials, 2007, 39(6): 588–599
6. Bajwa M S. Assesment of analytical procedures for designing metal buidlings for wind drift serviceability. Thesis for the Master's Degree. Blacksburg, VA: Virginia Polytechnic Institute and State University, 2010

7. Stamatopoulos G, Ermopoulos J. Experimental and analytical investigation of steel column bases. Journal of Constructional Steel Research, 2011, 67: 1341–1357
8. Verma A. Influence of column base fixity on lateral drift of gable frames. Thesis for the Master's Degree. Blacksburg, VA: Virginia Polytechnic Institute and State University, 2012
9. Amaral P M. Steel column bases under biaxial loading conditions. Thesis for the Master's Degree. Porto: University of Porto, 2014
10. Razzaghi J, Khoshbakht A. Numerical evaluation of column base rigidity. International Journal of Steel Structures, 2015, 15(1): 39–49
11. Nawar M T, Matar E B, Maaly H M, Alaaser A G, El-Zohairy A. Assessment of rotational stiffness for metallic hinged base plates under axial loads and moments. Buildings, 2021, 11(8): 368
12. He J C W, Clifton G C, Ramhormozian S, Hogan L S. Numerical and analytical study of pinned column base plate connections. Journal of Constructional Steel Research, 2023, 2023(204): 107846
13. Picard A, Beaulieu D. Behavior of a simple column base connection. Canadian Journal of Civil Engineering, 1985, 12(1): 126–136
14. Bajer M, Vild M, Barnat J, Holomek J. Influence of selected parameters on design optimisation of anchor joint. In: Proceedings of the 12th International Conference on Steel, Space and Composite Structures. Prague: Czech Technical University in Prague, 2014
15. Eurocode 3. Design of Steel Structures. Brussels: European Committee for Standardization, 2010
16. Kavoura F, Gencturk B, Dawood M. Reversed cyclic behavior of column-to-foundation connections in low-rise metal buildings. Journal of Structural Engineering, 2017, 143(9): 04017095
17. Kavoura F, Gencturk B, Dawood M. Evaluation of existing provisions for design of "pinned" column base-plate connections. Journal of Constructional Steel Research, 2018, 148: 233–250
18. Kavoura F, Gencturk B, Dawood M, Gurbuz M. Influence of base-plate connection stiffness on the design of low-rise metal buildings. Journal of Constructional Steel Research, 2015, 2015(115): 169–178
19. Kavoura F, Gurbuz M, Gencturk B, Dawood M, Hatch J, Navarro J. Moment–rotation behavior of "pinned" connections in low-rise metal buildings. In: Proceedings of Structures Congress 2014. Boston, MA: ASCE Structures Congress, 2014
20. AISC. Steel Construction Manual. Chicago, IL: American Institute of Steel Construction, 2016
21. Fisher J, Kloiber L. Base Plate and Anchor Rod Design, AISC Design Guide 1. Chicago, IL: American Institute of Steel Construction, 2006
22. Murray T M, Sumner E. Extended End-Plate Moment Connections: Seismic and Wind Applications, AISC Design Guide 4. Chicago, IL: American Institute of Steel Construction, 2003
23. Murray T M, Shoemaker W L. Flush and Extended Multiple-Row Moment End-Plate Connections, AISC/MBMA Design Guide 16. Chicago, IL: American Institute of Steel Construction/Metal Building Manufacturers Association, 2002
24. Consulting C. ATENA 3D User's Manual. 2017
25. Červenka V, Jendele L, Červenka J. ATENA Program Documentation, Part 1: Theory. Prague: Červenka Consulting, 2016